Ultrafast photodetection in an all-silicon chip enabled by two-photon absorption

J. Bravo-Abad,[a] E. P. Ippen, and M. Soljačić
Research Laboratory of Electronics, Massachusetts Institute of Technology, Cambridge, Massachusetts 02139, USA

(Received 27 March 2009; accepted 21 May 2009; published online 15 June 2009)

In this letter we theoretically demonstrate that by dramatically enhancing two-photon absorption, all-silicon optical microresonators can act as efficient photodetectors for light at telecom wavelengths. We illustrate this approach with two specific designs based on a ring resonator and a photonic crystal cavity. The proposed scheme is fully compatible with standard silicon complementary metal-oxide-semiconductor processing technology, and thus, could contribute to the development of chip-scale integrated photodetectors based exclusively on silicon. © *2009 American Institute of Physics*. [DOI: 10.1063/1.3155135]

One of the crucial steps toward the integration of microphotonics with silicon-based electronics resides in the development of efficient chip-scale photodetectors integrated on Si.[1–6] In this letter, we explore theoretically the feasibility of using two-photon absorption (TPA) (Ref. 7) to create on-chip ultrafast photodetectors exclusively from silicon. TPA in photoconductive semiconductors has been employed for the development of ultrafast autocorrelation and all-optical demultiplexing techniques.[8–11] However, to the best of our knowledge, none of these techniques as they stand allow implementing on-chip low-power high-speed photodetectors built onto a complementary metal-oxide-semiconductor (CMOS) compatible platform. We show that the dramatic enhancement of TPA that takes place in properly designed optical microresonators can enable efficient ultrafast photodetection in an all-silicon chip. Specifically, we analyze two particular designs based on a ring resonator and a photonic crystal (PC) cavity. Using detailed numerical calculations, we show that for bit rates of 1 Gbps, this class of photodetectors can reach an average ratio between the absorbed power due to TPA and the input optical power close to 20%. The performance of the proposed structures for higher bit rates is also discussed. The approach put forward in this manuscript allows envisioning an optoelectronic integrated device as the one illustrated in the main panel of Fig. 1(a).

We have applied a theoretical formalism based on a combination of a first order perturbation theory and a coupled-mode theory, similar to that described in Refs. 12 and 13. If the quantum efficiency of the photoconductivity is approximately 100%, the absorbed power due to TPA, $P_{\mathrm{abs}}(t)$, provides us with an accurate manner to evaluate the conversion efficiency between the light pulses and the electrical signals involved in our scheme.

Figures 1(b) and 1(c) display two possible physical implementations of the proposed photodetection scheme. The corresponding electromagnetic field profiles were computed with a finite-difference-time-domain method.[14] The results presented in this work corresponds to two-dimensional (2D) simulations. In order to obtain an accurate estimation of the performance of the actual three-dimensional (3D) counterparts of the considered structures, we have assumed that the electric field profile in the perpendicular direction to the plane shown in Figs. 1(b) and 1(c) is roughly the same as the mode profile computed for the 2D case; and that its extension in the third dimension is approximately $\lambda/4$. This fact does not affect the generality of our conclusions, since it is feasible to design 3D structures with 2D electric field cross sections very similar to the ones shown in this letter.[15] Figures 1(b) and 1(c) also show a possible configuration for the *p-i-n* junction embedded in each structure. In both cases, Q factors up to 10^5 can be reached, provided that the overlap between the doped regions and the resonant mode is minimal.[16,17] This value of Q includes also the effect of typical scattering losses due to the imperfections in the structure introduced during the fabrication process.

We start our analysis with a first set of calculations [see Figs. 2(a)–2(c)] in which a continuous train of 0.25 ns duration optical pulses is sent down the waveguide; the time interval between the pulses is 1 ns and the carrier frequency is the same as the resonant frequency of the microresonator. In the simulations we have assumed a thermal relaxation constant and an effective lifetime of the carriers of $\tau_{\mathrm{th}}=50$ ns and $\tau_{\mathrm{fc}}=80$ ps, respectively. These parameter values are characteristic for the class of microresonators considered here.[12,13,16,17] The optical absorbed power raises the temperature of the structure by $\Delta T(t)$, which in turn introduces a shift $\Delta n(t)$ of the refractive index of the microresonator. In this case, the heating of the microresonator is the dominant mechanism governing $\Delta n(t)$. For times $t \ll \tau_{\mathrm{th}}$ the increase of the temperature in the microresonator induced by each one of the subsequent pulses of the input train is added up, giving rise to the staircaselike profile of $\Delta n(t)$ displayed in the inset of Fig. 2(c). The plateau regions in this figure correspond to the time interval between the light pulses during which the structure does not have much time to shed its thermal energy via the thermalization with the environment. The growth of $\Delta n(t)$ saturates after approximately 100 ns [see Fig. 2(c)], while the maxima of $P_{\mathrm{abs}}(t)$ decrease with time, until reaching a steady-state value of 0.024 mW at ~100 ns (which corresponds to 16% of the maximum input power). The peak value chosen for $P_{\mathrm{in}}(t)$ ($P_{\mathrm{in}}^{\mathrm{max}}=0.15$ mW) in Figs. 2(a)–2(c) has been optimized to obtain the best possible ratio between the absorbed and input energies (i.e., the best conversion efficiency of the TPA process).

[a]Electronic mail: jbravo@mit.edu.

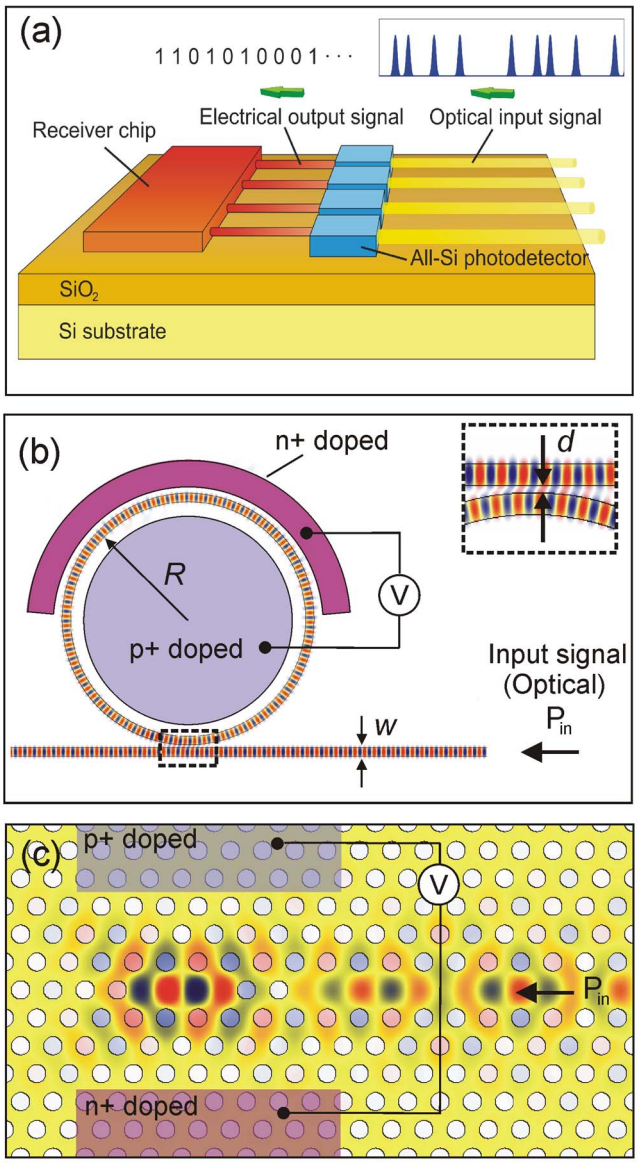

FIG. 1. (Color online) (a) Schematic of an on-chip integration of the photodetection scheme considered in this work. An arbitrary train of ultrafast light pulses is converted into an electric binary code (represented as a set of 1's and 0's). Panels (b) and (c) display two different designs analyzed in this manuscript, based on a ring resonator and a PC cavity, respectively. Yellow regions in both figures correspond to Si areas. In (b), $R=6\ \mu$m, $w=450$ nm, and $d=200$ nm; while in (c) the radius of the holes and the periodicity of the lattice are 90 and 330 nm, respectively. The electric and magnetic field profiles [pointing in the direction perpendicular to the page, see (b) and (c), respectively] for each structure are also shown; red (blue) correspond to the maximum (minimum) value of the corresponding field. Panels (b) and (c) also render possible configurations for the *p-i-n* junction embedded in each structure.

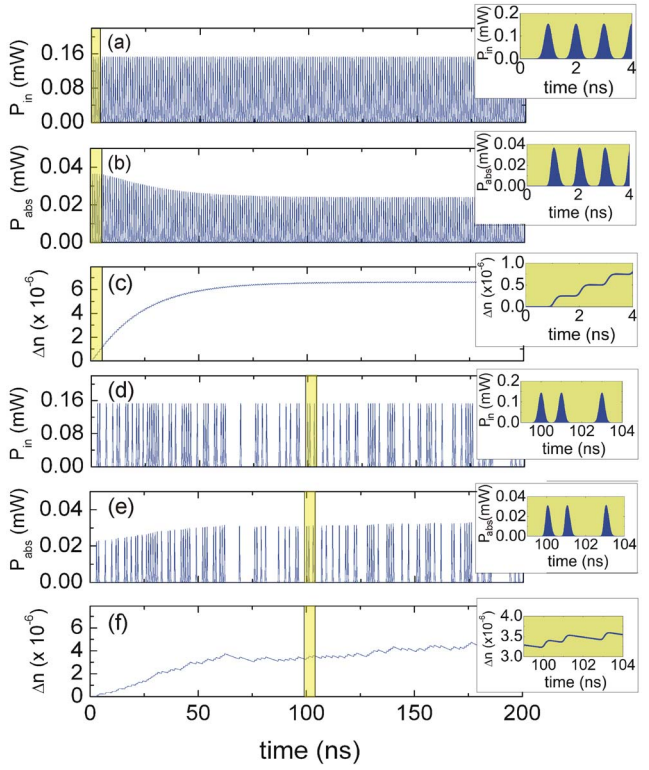

FIG. 2. (Color online) (a)–(c) display the time evolution of the input power (P_{in}), absorbed power (P_{abs}), and the variation of the refractive index of the microresonator (Δn), respectively, induced by a continuous train of 0.25 ns pulses illuminating the system shown in Fig. 1(c). $Q=10^5$ is assumed in these calculations. Panels (d), (e), and (f) have same magnitudes as in (a), (b), and (c), respectively, but now the external excitation consists in a pseudorandom train of pulses and the carrier frequency has been preshifted with respect to the resonant frequency of the microresonator. Inset of each panel shows an enlarged view of the yellow shaded area of the corresponding main figure.

Next, we analyze the response of the system shown in Fig. 1(c) pseudorandom train of 0.25 ns pulses. Pseudorandom sequences of signals are routinely employed to test electronic integrated circuits. The results of the corresponding computations are displayed in Figs. 2(d)–2(f). In these simulations, we have assumed the same physical parameters as those used in Figs. 2(a)–2(c). The physical description of the behavior observed in Figs. 2(d)–2(f) is similar to the one given above for the case of a continuous train of pulses. However, in contrast to the results shown before, we have now introduced a preshift $\Delta\omega$ into the frequency of the input signal, so the signal carrier frequency is not the same as the resonant frequency of the microresonator. We have found that the absorbed power can be improved by choosing $\Delta\omega=-\omega\Delta n_c$, where Δn_c is the steady-state value of the $\Delta n(t)$ obtained from the set of simulations corresponding to a continuous train of pulses with no frequency preshift with respect to the resonant frequency of the microresonator [see Figs. 2(a)–2(c)]. The response of the structure based on the Si ring microresonator shown in Fig. 1(b) is qualitatively the same as the one described above for the PC cavity. However, as we show below, the larger modal volume of the ring resonator compared to the modal volume of the PC cavity causes a reduction of the conversion efficiency.

Figures 3(a) and 3(b) display the dependence of the energy absorbed per pulse, E_{abs}, as a function of the energy of each input pulse, E_{in}, for operating bit rates of 1 Gbps and 10 Gbps, respectively. The corresponding results for the case of the ring resonator shown in Fig. 1(b) are displayed in Figs. 3(c) and 3(d). The simulation for each bit rate was performed assuming the maximum possible value of Q that allows operation at the considered bit rate (note that, for instance, the duration of the light pulses has to be reduced from 0.25 to 0.025 ns when the bit rate is increased from 1 to 10 Gbps). Dashed green lines in each figure indicate the optimal operating point for each case. In this optimal regime, the response of the photodetector does not depend much ($<0.1\%$) on the input signal pattern. Thus, in the case of the

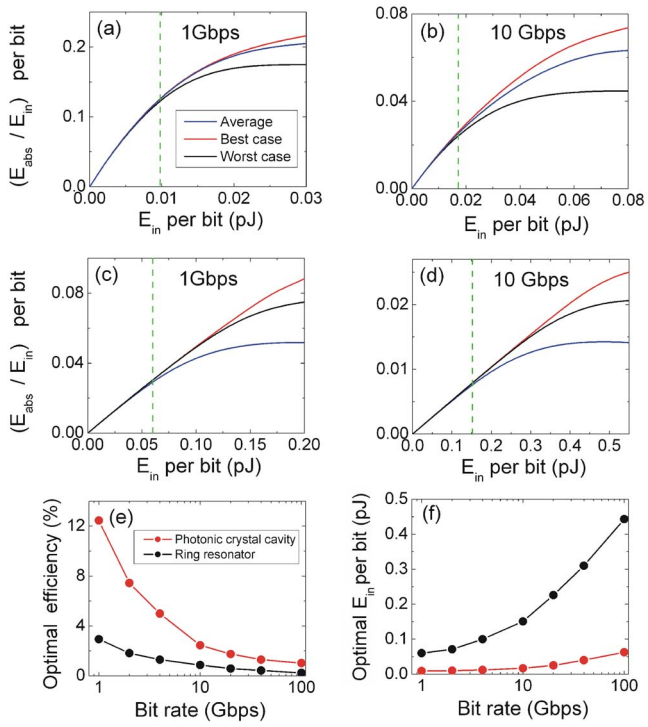

FIG. 3. (Color online) Panels (a) and (b) show the ratio between the absorbed and the input energy for the PC microcavity displayed in Fig. 1(c), operating at 1 and 10 Gbps, respectively. The results for each bit rate have been computed assuming the maximum possible value of the Q factor that allows the considered bit rate. Panels (c) and (d) render the same magnitudes as (a) and (b), but in this case computed for the ring resonator structure shown in Fig. 1(b). Panels (e) and (f) display the results for the optimal efficiency and the optimal energy per bit [indicated as dashed green lines in panels (a)–(d)] as a function of the corresponding bit rate. Red and black dots correspond to the structures of Figs. 1(c) and 1(b), respectively.

PC microcavity, for $Q=10^5$ and a bit rate of 1 Gbps, a value of $E_{\mathrm{abs}}/E_{\mathrm{in}}$ of 0.12 (i.e., conversion efficiency of 12%) can be reached for input pulse energies of 0.010 pJ without any significant difference between the most and the least absorbed pulses of the pseudorandom sequence of pulses. This value of the conversion efficiency is reduced to 3% for the case of the ring resonator, while in this case the input pulse energy increases to 0.06 pJ. Also note that both in the case of the PC cavity and the ring resonator, the ratio between the absorbed power due to TPA and the input optical power do not have large variations over almost half an order of magnitude; which could be of interest for optical interconnects, where signal energies entering a given device are often known. Figures 3(e) and 3(f) display the dependence of the optimal efficiency and optimal input energy per bit, respectively, as a function of the bit rate for the two structures displayed in Figs. 1(b) and 1(c). The minimum detectable optical power by the class of photodetectors introduced in this letter can be characterized by means of the noise equivalent power (NEP).[18] Assuming operation at room temperature, it can be shown that the value of NEP for the systems shown in Figs. 1(b) and 1(c) is approximately 3.6×10^{-2} pW/Hz$^{1/2}$. Consequently, the minimum absorbed powers P_{abs} required for operating bandwidths of 1 and 100 GHz are 1.14 and 11.4 nW, respectively. Both values for P_{abs} are several orders of magnitude below the optimal absorbed powers that can be deduced from Figs. 3(e) and 3(f). Therefore, we expect the TPA-based photodetection approach proposed here to be feasible at room temperature for the whole range of bit-rates displayed in Fig. 3. Also note that the value for NEP we obtain is similar to the one characterizing direct-gap photodiodes currently used in high-bit-rate optical communications at 1550 nm.[18]

To conclude, we have proposed an approach to all-silicon photodetection based on the enhancement of TPA in properly designed optical microresonators. The scheme demonstrated in this work can help in developing practical ultrafast all-silicon photodetectors that can be integrated onto a CMOS platform.

The authors thank Professor John D. Joannopoulos, Professor Leslie Kolodziejski, and Dr. Morris Kesler for valuable discussions. This work was supported by the MRSEC Program of the National Science Foundation under award number DMR-0819762, by AFOSR Grant No. FA9550-07-1-0014, and by the U.S. Army Research Office through the Institute for Soldier Nanotechnologies under Contract No. W911NF-07-D-0004.

[1] *Silicon Photonics*, edited by L. Pavesi and D. J. Lockwood (Springer, Berlin, 2004).
[2] *Silicon Photonics: The State of the Art*, edited by G. T. Reed (Wiley, Chichester, 2008).
[3] J. Liu, J. Michel, W. Giziewicz, D. Pan, K. Wada, D. Cannon, L. C. Kimerling, J. Chen, F. O. Ilday, F. X. Kartner, and J. Yasaitis, Appl. Phys. Lett. **87**, 103501 (2005).
[4] L. Colace,G. Masini, A. Altieri, and G. Assanto, IEEE Photonics Technol. Lett. **18**, 1094 (2006).
[5] T. Yin, R. Cohen, M. Morse, G. Sarid, Y. Chetrit, D. Rubin, and M. J. Paniccia, Opt. Express **15**, 13965 (2007).
[6] L. Chen, P. Dong, and M. Lipson, Opt. Express **16**, 11513 (2008).
[7] R. W. Boyd, *Nonlinear Optics*, 2nd ed. (Academic, San Diego, 2003).
[8] Y. Takagi, T. Kobayashi, K. Yoshihara, and S. Imamura, Opt. Lett. **17**, 658 (1992).
[9] B. C. Thomsen, L. P. Barry, J. M. Dudley, and J. D. Harvey, Electron. Lett. **34**, 1871 (1998).
[10] T. K. Liang, H. K. Tsang, I. E. Day, J. Drake, A. P. Knights, and M. Asghari, Appl. Phys. Lett. **81**, 1323 (2002).
[11] H. Folliot, M. Lynch, A. L. Bradley, L. A. Dunbar, J. Hegarty, J. F. Donegan, L. P. Barry, J. S. Roberts, and G. Hill, Appl. Phys. Lett. **80**, 1328 (2002).
[12] P. Barclay, K. Srinivasan, and O. Painter, Opt. Express **13**, 801 (2005).
[13] T. J. Johnson, M. Borselli, and O. Painter, Opt. Express **14**, 817 (2006).
[14] A. Taflove and S. C. Hagness *Computational Electrodynamics: The Finite-Difference Time-Domain Method*, 3rd ed. (Artech, Norwood, 2005); A. Farjadpour, D. Roundy, A. Rodriguez, M. Ibanescu, P. Bermel, J. D. Joannopoulos, S. G. Johnson, and G.W. Burr, Opt. Lett. **31**, 2972 (2006).
[15] M. L. Povinelli S. Johnson, S. Fan, and J. D. Joannopoulos, Phys. Rev. B **64**, 075313 (2001).
[16] Q. Xu, B. Schmidt, S. Pradhan, and M. Lipson, Nature (London) **435**, 325 (2005).
[17] T. Tanabe, M. Notomi, S. Mitsugi, A. Shinya, and E. Kuramochi, Opt. Lett. **30**, 2575 (2005); T. Tanabe, H. Taniyama, and M. Notomi, J. Lightwave Technol. **26**, 1396 (2008).
[18] H. Kolimbiris, *Fiber Optics Communications* (Pearson/Prentice Hall, Saddle River, 2004).